A sodium-channel mutation causes isolated cardiac conduction disease

Hanno L. Tan*†‡, Margreet T. E. Bink-Boelkens‡§, Connie R. Bezzina*‖, Prakash C. Viswanathan†, Gertie C. M. Beaufort-Krol§, Peter J. van Tintelen¶, Maarten P. van den Berg#, Arthur A. M. Wilde* & Jeffrey R. Balser†

** The Experimental and Molecular Cardiology Group, and ‖ Department of Clinical Genetics, Academic Medical Center, University of Amsterdam, 1105 AZ Amsterdam, The Netherlands*
§ Department of Pediatric Cardiology, Beatrix Children's Hospital, 9700 RB Groningen, The Netherlands
¶ Department of Medical Genetics, University Hospital, 9700 RB Groningen, The Netherlands
 # Department of Cardiology, University Hospital, 9700 RB Groningen, The Netherlands
† Departments of Anesthesiology and Pharmacology, Vanderbilt University School of Medicine, Nashville, Tennessee 37232, USA
‡ These authors contributed equally to this work

Cardiac conduction disorders slow the heart rhythm and cause disability in millions of people worldwide. Inherited mutations in *SCN5A*, the gene encoding the human cardiac sodium (Na^+) channel, have been associated with rapid heart rhythms that occur suddenly and are life-threatening[1–3]; however, a chief function of the Na^+ channel is to initiate cardiac impulse conduction. Here we provide the first functional characterization of an *SCN5A* mutation that causes a sustained, isolated conduction defect with pathological slowing of the cardiac rhythm. By analysing the *SCN5A* coding region, we have identified a single mutation in five affected family members; this mutation results in the substitution of cysteine 514 for glycine (G514C) in the channel protein. Biophysical characterization of the mutant channel shows that there are abnormalities in voltage-dependent 'gating' behaviour that can be partially corrected by dexamethasone, consistent with the salutary effects of glucocorticoids on the clinical phenotype. Computational analysis predicts that the gating defects of G514C selectively slow myocardial conduction, but do not provoke the rapid cardiac arrhythmias associated previously with *SCN5A* mutations.

We have studied a family who came to medical attention when the proband, a 3-yr-old girl (pedigree: Fig. 1a, III-2), experienced episodes of fainting during a febrile illness. Her 12-lead electrocardiogram (ECG) showed characteristics of slow conduction throughout the atria and ventricles, including broad P waves, PR interval prolongation, and a wide QRS complex (Fig. 1c). Continuous heart rhythm monitoring (Fig. 1d) revealed episodes of severe bradycardia (25 beats min^{-1}), which might arise from a reduced firing rate by the sinus node (native cardiac pacemaker), or from suppressed conduction through atrial tissues in the vicinity of the sinus node. During these slow periods, the cardiac rhythm was maintained by infrequent atrioventricular nodal 'escape' impulses (Fig. 1d, arrows).

The conduction disturbance persisted after the febrile illness resolved, and we determined no evidence of structural heart disease (echocardiography) or systemic diseases associated with conduction defects in children (viral infections, auto-immune or Lyme disease, thyroid dysfunction). Therapeutic intervention with a dual-chamber pacemaker was initially limited by inability to pace the atrium (maximal stimulus: 10 V, 1 ms); however, this difficulty resolved with 1 week of empirical steroid treatment (given originally to exclude an inflammatory aetiology for the conduction disturbance), which comprised intravenous methylprednisolone followed by oral prednisone.

During the 4 years following diagnosis, the proband has

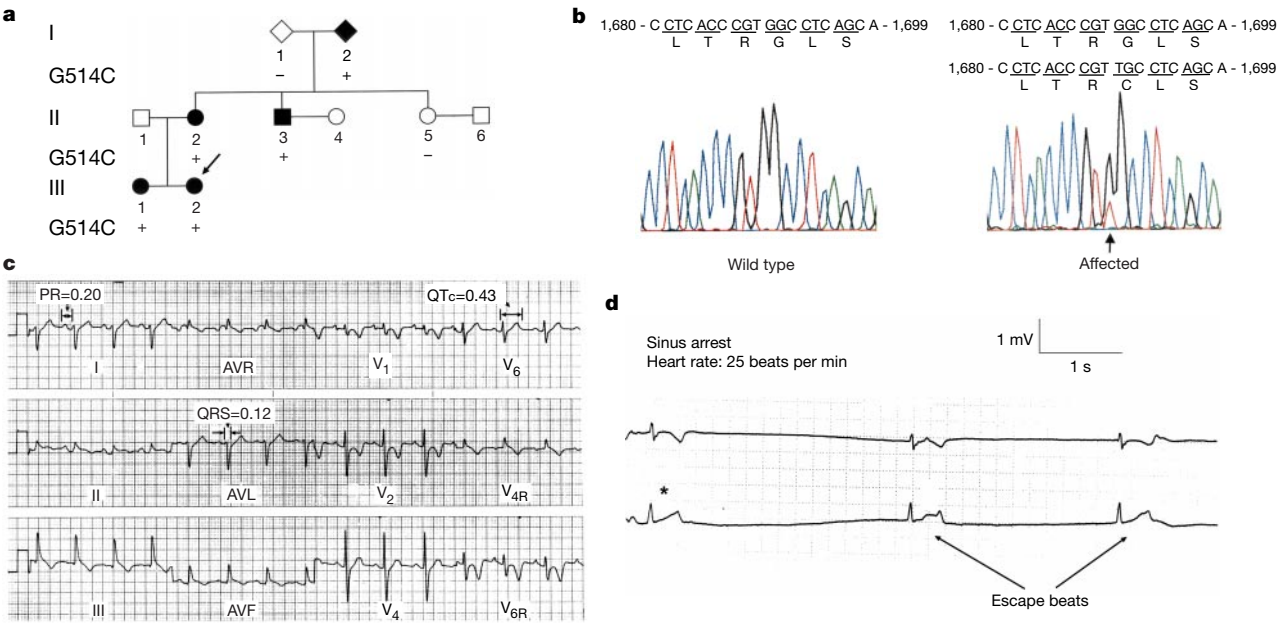

Figure 1 Genotype and ECG phenotype. **a**, Pedigree (arrow, proband) shows individuals consenting to SSCP analysis. +, carrier; –, non-carrier; square, male; circle, female; diamond, anonymous; filled symbol, conduction disease. **b**, Sequence identification of a G to T transversion (arrow) of one *SCN5A* allele in an affected individual (both alleles shown), causing replacement of glycine 514 by cysteine (G514C). **c**, Twelve-lead ECG of proband, indicating sinus rhythm with prolonged PR and QRS intervals (age-corrected normal values, 0.08–0.16 s and 0.03–0.07 s, respectively)[24] and a rightward QRS axis shift, but no signs of Brugada or long QT syndrome. The P wave and QRS interval reflect atrial and ventricular conduction, respectively, and the PR interval reflects atrioventricular conduction. The QTc reflects ventricular repolarization, and is the QT interval (indicated on the figure) corrected for heart rate (QT/cycle length$^{0.5}$). **d**, Rhythm strip of proband shows typical bradycardia episode. The pauses after the last sinus beat (asterisk) are terminated by escape beats from a subsidiary pacemaker.

© 2001 Macmillan Magazines Ltd

continuously required dual-chamber pacing. Examination of the family revealed nearly identical findings in a 6-yr-old sister (Fig. 1a, III-1). She also underwent pacemaker implantation with episodes of non-capture that reproducibly resolved with corticosteroid therapy. Three other family members (Fig. 1a, I-2, II-2, II-3) with no structural heart disease had ECG evidence of conduction slowing (prolonged PR and QRS intervals), but did not experience bradycardia or require pacemaker implantation. Single-strand conformation polymorphism (SSCP) analysis of the coding region of *SCN5A* identified an aberrant conformer in exon 12 in all five clinically affected family members. DNA sequencing in each of these individuals revealed a G to T transversion at the first nucleotide of codon 514 (Fig. 1b), resulting in the replacement of glycine by cysteine (G514C). The mutation was absent in 200 alleles from unaffected control individuals. In the proposed topology of the voltage-gated Na^+ channel[4], this mutation is located intracellularly in the I–II interdomain linker.

To identify a functional mechanism for the slow-conducting phenotype, we expressed wild-type and G514C Na^+ channels in tsA201 cells to allow voltage-clamp measurements. On depolarization, Na^+ channels rapidly activate (open) and inactivate, producing a transient inward whole-cell current (I_{Na}; Fig. 2a). G514C I_{Na} and wild-type I_{Na} were similar in size (Fig. 2, legend), suggesting that the mutation did not change expression; however, G514C I_{Na} decayed more rapidly than wild-type I_{Na} (Fig. 2a). The decay rate was bi-exponential (Fig. 2a), and the predominant, more rapid time constant (τ_{fast}) was reduced by the mutation (Fig. 2b, −10 to 20 mV, $P < 0.05$), consistent with hastened inactivation of open channels. In addition, the magnitude of I_{Na} was shifted by +10 mV on the voltage axis (Fig. 2c, $P = 0.0003$), indicating a modified voltage dependence of activation. Both gating defects would reduce the I_{Na} available to support cardiac impulse conduction.

Further studies indicated that there were counterbalancing G514C gating effects that would increase the availability of I_{Na} (Figs 3 and 4a). Although mutant open-state inactivation was hastened (Fig. 2a, b), Na^+ channels also inactivate at membrane potentials below the opening threshold (so-called 'closed-state' inactivation)[5]. Examination of steady-state G514C availability at potentials negative to the opening threshold (Fig. 3a) revealed a +7 mV shift ($P = 0.003$ versus wild type), suggesting that closed-state inactivation was reduced.

A more detailed kinetic analysis using a variable-duration prepulse (Fig. 3b) found no significant change in the inactivation time constant (−90 mV: $\tau = 75 \pm 5$ ms for G514C versus 69 ± 8 ms for wild type; not significant), but the extent of G514C closed-state inactivation was reduced greatly (Fig. 3b, legend). Hence, the results in Fig. 3 suggest that the mutant inactivated state (once occupied)

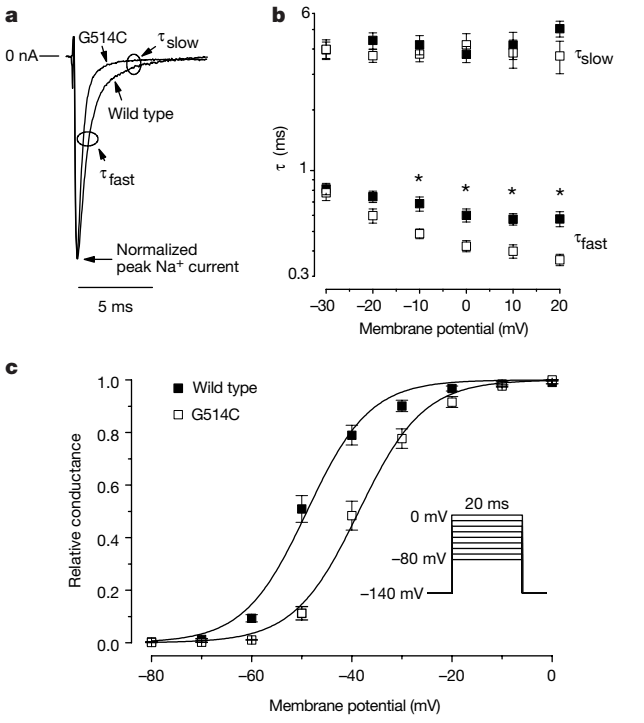

Figure 2 G514C gating effects that reduce I_{Na} availability. **a**, Wild-type and G514C I_{Na} transients are normalized to illustrate differences in decay rate. Peak I_{Na} density at 0 mV: wild-type ($n = 6$), 0.76 ± 0.10 nA pF^{-1}; G514C ($n = 7$), 0.56 ± 0.08 nA pF^{-1} (not significant). **b**, I_{Na} decay was fitted by the function $y = A_1(1 - \exp[-t/\tau_{fast}]) + A_2(1 - \exp[-t/\tau_{slow}])$. τ_{fast}, τ_{slow} are plotted for wild type ($n = 6$) and G514C ($n = 7$) (*$P < 0.05$ versus wild type). At −10 mV: wild type, $A_1 = 0.89 \pm 0.03$, $A_2 = 0.11 \pm 0.03$; G514C, $A_1 = 0.94 \pm 0.01$, $A_2 = 0.06 \pm 0.01$ (not significant). **c**, Voltage-dependence of activation. Relative conductance was fitted to a Boltzmann function $y = [1 + \exp\{(V - V_{1/2})/k_B\}]^{-1}$. Wild type ($n = 6$) $V_{1/2} = -48.6 \pm 1.2$ mV, $k_B = 6.1 \pm 0.8$; G514C ($n = 7$) $V_{1/2} = -38.5 \pm 1.4$ mV ($P = 0.0003$ versus wild type), $k_B = 6.1 \pm 0.3$. At 32 °C: G514C ($n = 5$; not shown) $V_{1/2} = -37.9 \pm 3.2$ mV (not significant versus 22 °C), $k_B = 5.6 \pm 0.9$ (not significant versus 22 °C).

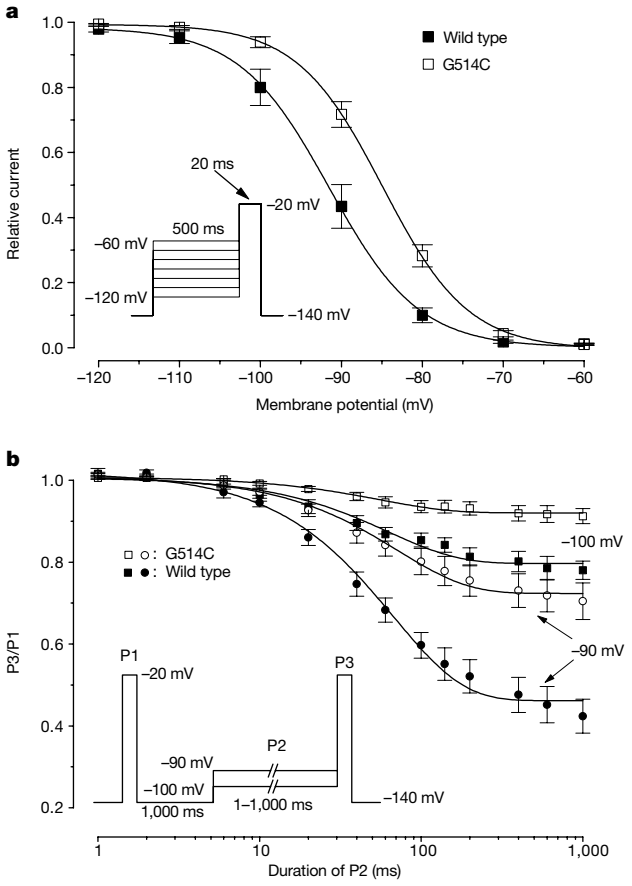

Figure 3 G514C gating effects that increase I_{Na}. **a**, The voltage dependence of steady-state availability (protocol shown, see Methods), fitted by a Boltzmann function (see Fig. 2c). Wild type ($n = 6$) $V_{1/2} = -92.0 \pm 1.7$ mV, $k_B = 5.4 \pm 0.3$; G514C ($n = 7$) $V_{1/2} = -85.1 \pm 0.9$ ($P = 0.003$ versus wild type), $k_B = 5.2 \pm 0.3$. At 32 °C: G514C ($n = 5$; not shown) $V_{1/2} = -84.1 \pm 2.1$ (not significant versus 22 °C), $k_B = 5.5 \pm 0.4$ (not significant versus 22 °C). **b**, Closed-state inactivation at membrane potentials near V_{rest} (protocol shown). Solid lines indicate least-squares fits to the function $y = y_0 + A\exp(-t/\tau)$. At −90 mV: wild type ($n = 6$) $\tau = 69 \pm 8$ ms, $A = 0.56 \pm 0.05$; G514C ($n = 7$) $\tau = 75 \pm 5$ ms (not significant versus wild type), $A = 0.28 \pm 0.04$ ($P < 0.01$ versus wild type). At −100 mV: wild type $\tau = 70 \pm 13$ ms, $A = 0.21 \pm 0.02$; G514C $\tau = 56 \pm 6$ ms (not significant versus wild type), $A = 0.08 \pm 0.01$ ($P < 0.001$ versus wild type).

© 2001 Macmillan Magazines Ltd

was partly destabilized. Fig. 4a shows speeded recovery of inactivated G514C channels during hyperpolarization, further indicating that the mutant inactivated state was destabilized. Bath-applied reduced glutathione (1 mM, $n = 7$) did not modify G514C gating (data not shown), suggesting that these diverse functional defects (Figs 2–4) did not result from cysteine oxidation, but rather from allosteric effects caused by residue substitution that involve several gating domains.

Given the clinical improvement of two patients receiving steroid therapy, we analysed the effects of steroids on G514C gating. We incubated G514C and wild-type cells with dexamethasone (1 μM) for 48 h after transfection. Dexamethasone partially rescued the mutation-induced shift in the voltage dependence of activation (Fig. 4b, left), but did not change G514C inactivation (Fig. 4b, right) and had no effect on wild-type gating (Fig. 4b). There was no effect of steroid pretreatment on I_{Na} density (Fig. 4b, legend) or on the rate of I_{Na} decay. Acute exposure of G514C to 1 μM dexamethasone ($\leq$ 30 min) through either the intracellular (pipette) or extracellular solution had no effects ($n = 6$ in each case; data not shown),

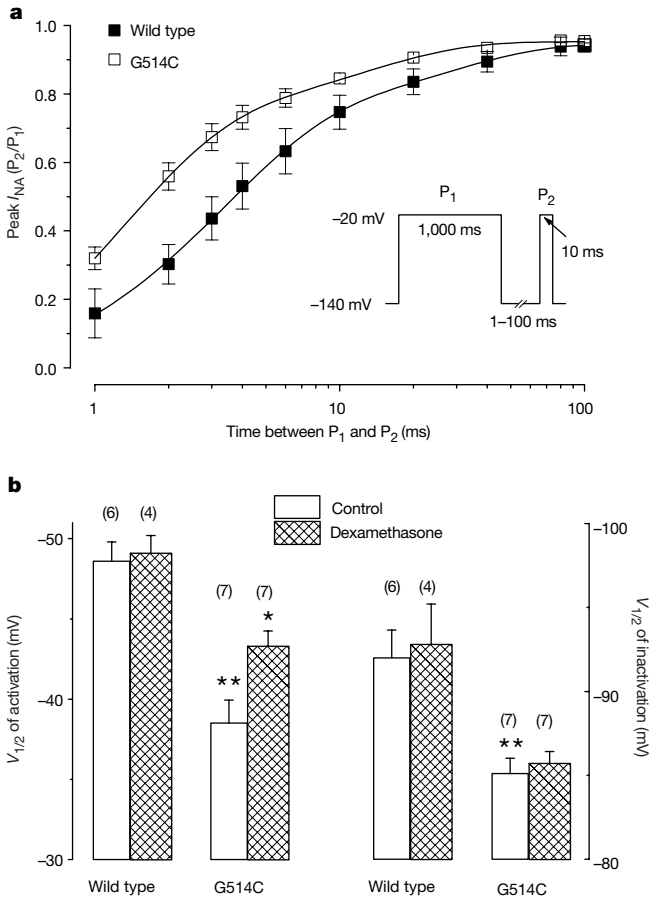

Figure 4 G514C inactivated-state instability, and steroid effects on gating. **a**, Recovery from inactivation (protocol shown, see Methods), fitted by the function $y = y_0 + A_1(1 - \exp[-t/\tau_1]) + A_2(1 - \exp[-t/\tau_2])$. Wild type ($n = 5$) $\tau_1 = 4.5 \pm 0.2$ ms, $\tau_2 = 81.7 \pm 17.3$ ms, $A_1 = 0.82 \pm 0.04$, $A_2 = 0.18 \pm 0.03$; G514C ($n = 7$) $\tau_1 = 2.1 \pm 0.4$, $\tau_2 = 48.0 \pm 6.2$, $A_1 = 0.84 \pm 0.01$, $A_2 = 0.15 \pm 0.01$ (τ_1, $P = 0.007$ versus wild type). **b**, Effects of dexamethasone on G514C gating. Plotted are $V_{1/2}$ for activation (left ordinate) and inactivation (right ordinate) of wild type and G514C in the absence and presence of dexamethasone. G514C caused depolarizing shifts (**$P < 0.05$ versus wild type) in $V_{1/2}$ of activation and inactivation. Dexamethasone partially reversed the activation effect (*$P < 0.05$), but did not change inactivation gating or I_{Na} density (0 mV) of G514C (control, 0.56 ± 0.08 nA pF^{-1}, $n = 7$; dexamethasone, 0.46 ± 0.05, $n = 7$; not significant) or wild type (control, 0.76 ± 0.10, $n = 6$; dexamethasone, 0.62 ± 0.05, $n = 4$; not significant).

suggesting that the selective effect on G514C activation gating did not result from a direct interaction between dexamethasone and the Na^+ channel. The method whereby steroids influenced G514C gating remains speculative, but the requirement for sustained exposure suggests that the mechanisms involve channel synthesis, post-translational modification, or modified expression of auxiliary subunits.

Studies of Na^+-channel function suggest that Brugada syndrome mutations reduce I_{Na}, hastening epicardial repolarization and causing idiopathic ventricular fibrillation[6–8], whereas mutations that evoke the long QT syndrome (LQT3) cause excessive I_{Na}, delaying repolarization and causing a distinctive ventricular tachyarrhythmia (Torsades de Pointes)[1,2,9]. G514C evokes gating effects reminiscent of both syndromes (an activation gating shift that tends to reduce I_{Na}, and destabilized inactivation that tends to increase I_{Na}), but G514C carriers do not exhibit characteristic features of either LQT3 or Brugada syndrome (Fig. 1c). We thought that the 'balance' of the opposing G514C gating effects may produce isolated conduction slowing without evoking the Brugada syndrome or LQT3 repolarization defects.

We used computational studies to examine a model fibre that recapitulates layer-specific cardiac action-potential characteristics and cell-to-cell conduction[10]. First, we examined whether the G514C gating defects could reproduce the clinically observed conduction delay. Experimental studies[11,12] indicate that increasing the voltage difference (ΔV) between the cardiac resting potential (V_{rest}) and the Na^+-channel activation (opening) threshold decreases conduction velocity. We explored the isolated effect of reducing ΔV by shifting the voltage dependence of activation (as in G514C; Fig. 2c), rather than by depolarizing V_{rest} (with external K^+ in the experimental studies)[11,12]. The model simulations (Fig. 5a) show a striking decrease in conduction velocity (left ordinate) as activation gating is shifted. There is also a marked increase in the minimum voltage stimulus necessary to support conduction through the fibre (right ordinate). The second observation might provide a rationale for the relative inexcitability of G514C carriers to pacemaker stimulation, and might also link the dexamethasone effects on G514C activation (Fig. 4b) to the improved pacemaker response with steroid therapy.

Given that these simulations linked the G514C activation gating defect to conduction slowing, we considered how the additional inactivation gating defect (Fig. 3a) would influence the model fibre. Epicardial cells exhibit a potassium current (I_{to}) that inscribes a 'notch' in the early plateau phase of the action potential (Fig. 5b, left). This repolarizing force renders the action potential 'sensitive' to factors that reduce I_{Na} (ref. 13). As such, Na^+-channel mutations that reduce I_{Na} (that is, Brugada syndrome T1620M)[3] severely shorten the action potential in the epicardium, but not in the inner-cell layers (Fig. 5b, middle). This layer-specific effect evokes a gradient in membrane potential from the epicardial to inner-cell layers, and may cause transmural current flow sufficient to induce the ECG changes and ventricular arrhythmias of Brugada syndrome[14,15]. Although G514C also exhibits gating defects that reduce I_{Na} (Fig. 2), the mutation destabilizes closed-state inactivation at the resting membrane potential (Fig. 3a, b), an effect that should increase Na^+-channel availability. Incorporating these

Table 1 Transverse conduction velocity

	Wild-type	Brugada syndrome (T1620M)	Conduction disease (G514C)	G514C + dexamethasone
Endocardial	22.8	18.8 (18%)	20.0 (12%)	21.0 (8%)
Midmyocardial	21.4	17.0 (21%)	18.4 (14%)	19.5 (9%)
Epicardial	20.4	15.8 (23%)	17.3 (15%)	18.4 (10%)

Calculated transverse conduction velocities (cm s^{-1}) between 10 cells in epicardial, endocardial and midmyocardial regions. The percentage change from wild-type value is given in parentheses. Simulation conditions were those described in Fig. 5b, including the heterozygous state for T1620M and G514C.

© 2001 Macmillan Magazines Ltd

opposing gating effects into the model restored normal epicardial action-potential duration (Fig. 5b, right) while slowed conduction velocity persisted (Table 1), consistent with the clinical phenotype.

An activation gating defect similar to G514C (Fig. 2c) has been identified in T1620M[6], consistent with clinical reports indicating that Brugada syndrome patients have marked abnormalities in ventricular conduction[16,17]. In fact, the modelling results predict that destabilized closed-state inactivation gating of G514C may attenuate the ventricular conduction delay (Table 1, compare G514C with T1620M). In the three adult G514C carriers, the QRS intervals were 120 ms (Fig. 1a, pedigree I-2), 106 ms (II-2) and 110 ms (II-3)—values at the upper limit of normal—whereas the QRS intervals in Brugada syndrome patients are generally more prolonged. In the original report describing Brugada syndrome[16], the QRS intervals were well above 120 ms in 6 out of 8 patients, and were 120 ms in the other 2 patients.

Analysis of the ECGs of G514C carriers indicates that steroid therapy improves not only atrial, but also ventricular conduction. In both children (Fig. 1a, III-1, III-2), the QRS duration during spontaneously conducting (non-paced) periods was shorter (by ~40 ms) after steroid treatment. Moreover, incorporating the antagonistic effect of dexamethasone on the G514C-induced activation shift (Fig. 4b) enhanced, but did not fully correct, the model fibre conduction velocity (Table 1) as seen clinically. Conduction velocity in the myocardium is heavily determined by the maximum rate of rise of the action potential upstroke (Fig. 5b, boxed area on wild-type and G514C action potentials). This portion of the action potential is redrawn (Fig. 5b, inset) using an expanded time base to provide intuitive insight into how the activation gating effects of G514C and dexamethasone alter the conduction velocity in the model fibre. For the simulations shown, epicardial dV/dt_{max} was 306 V s^{-1} for wild type, but was only 242 V s^{-1} for G514C. The reduced activation shift associated with dexamethasone treatment of G514C yielded an intermediate dV/dt_{max} value (279 V s^{-1}), consistent with the model-predicted conduction velocities (Table 1).

The number of gating defects associated with the G514C mutation provides a biophysical mechanism for the conduction defects observed in this family. At the same time, *SCN5A* mutations have been identified in two families with inherited conduction disease that might, on the basis of rather large deleted segments, produce entirely non-functional Na^+ channels[18]. Although functional data are not available for these mutations, the lack of a tachyarrhythmia phenotype indicates that 'modifier' genes, allele penetrance and/or developmental factors may also influence the relationship between conduction disease and Na^+-channel function. Nonetheless, the G514C channel provides new evidence that Na^+-channel gating dysfunction can produce isolated conduction disease, with pathological slowing of the heart rhythm. This inherited lesion suggests a biophysical framework for understanding how the diverse functional behaviour of a single ion channel may evoke a spectrum of

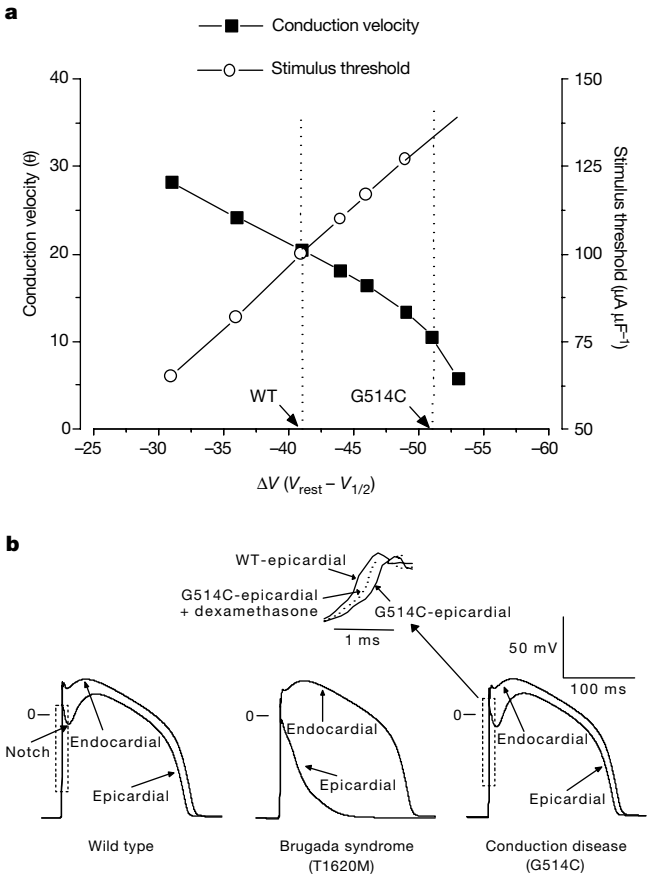

Figure 5 Action potential propagation in a model fibre. **a**, Model-predicted values for conduction velocity and stimulus magnitude required to support conduction, as a function of voltage dependence of activation. ΔV, difference (in mV) between activation $V_{1/2}$ and V_{rest} (about –90 mV). Dotted lines indicate ΔV for wild-type (WT) and G514C channels. **b**, Simulated endocardial and epicardial action potentials. Middle and Right panels simulate the heterozygous condition (50:50 mixture of mutant and wild-type channels). Left, wild-type action potentials; the epicardial 'notch' due to I_{to} is indicated. Middle, T1620M; $V_{1/2}$ of activation shifted +10 mV and I_{Na} decay hastened to one-half of wild-type value (ref. 6). Right, G514C; $V_{1/2}$ of activation shifted +10 mV (Fig. 2c), I_{Na} decay speeded to two-thirds of wild-type value (Fig. 2a), and $V_{1/2}$ of inactivation shifted +7 mV (Fig. 3a). **b**, Inset, action potential upstroke (boxed regions on wild-type and G514C action potentials) shown on an expanded time base to illustrate dV/dt_{max}. Dotted line indicates predicted G514C dV/dt_{max} in dexamethasone, where the G514C activation $V_{1/2}$ shift is reduced from +10 mV to +5 mV (Fig. 4b).

© 2001 Macmillan Magazines Ltd

deranged cardiac excitability, from conduction disease to sudden cardiac death. □

Methods

Sequence analysis, mutagenesis and transfection

The entire coding region of *SCN5A* was screened by SSCP and direct sequence analysis as described[19], and site-directed mutagenesis was performed on *SCN5A* complementary DNA cloned into the green fluorescent protein (GFP) expression vector pCGI (ref. 20) as described[21]. Cultured cells (tsA201) were co-transfected with a 5:1 molar ratio of the Na^+-channel β_1 subunit (provided by A. George, Vanderbilt University).

Electrophysiology

Unless otherwise indicated, I_{Na} was recorded at room temperature (22 °C) to optimize voltage-clamp control using established recording conditions[7]. For all voltage-clamp experiments, the pipette solution contained (in mM): NaF 10, CsF 110, CsCl 20, EGTA 10 and HEPES 10 (pH 7.35 with CsOH), and the bath solution contained: NaCl 145, KCl 4, $CaCl_2$ 1.8, $MgCl_2$ 1, HEPES-NaOH pH 7.35. For voltage-dependent activation (Fig. 2c), relative conductance was calculated by dividing the peak I_{Na} at each clamp potential by the driving force (clamp voltage minus measured reversal potential), then normalizing to the value at 0 mV. For voltage-dependent inactivation (Fig. 3a), relative currents were calculated by normalizing peak I_{Na} (elicited by depolarization to −20 mV) to the value recorded after holding at the most negative (−120 mV) conditioning voltage. The rate of development of closed-state inactivation (Fig. 3b) was analysed using variable duration pre-pulses to −90 or −100 mV. The kinetics of recovery from inactivation (Fig. 4a) were assessed using a three-pulse clamp protocol. The ratio of the peak I_{Na} elicited by the P_2 pulse, relative to the P_1 pulse, was plotted as a function of the intervening recovery interval at −140 mV.

Action potential simulations

The Luo–Rudy model[10,22,23] of a mammalian ventricular myocyte action potential provided the basis for the action potential simulations (Fig. 5), with I_{to} added as described[6]. A one-dimensional fibre[10] consisting of endocardial (cells 1–80), midmyocardial (81–110), and epicardial (111–190) cells was used to mimic *in vivo* conditions. A stimulus was applied to cell no. 1 to simulate normal endocardial to epicardial impulse propagation.

Received 22 November; accepted 21 December 2000.

1. Wang, Q. *et al. SCN5A* mutations associated with an inherited cardiac arrhythmia, long QT syndrome. *Cell* **80,** 805–811 (1995).
2. Bennett, P. B., Yazawa, K., Naomasa, M. & George, A. L. Molecular mechanism for an inherited cardiac arrhythmia. *Nature* **376,** 683–685 (1995).
3. Chen, Q. *et al.* Genetic basis and molecular mechanism for idiopathic ventricular fibrillation. *Nature* **392,** 293–296 (1998).
4. Noda, M. *et al.* Expression of functional sodium channels from cloned cDNA. *Nature* **322,** 826–828 (1986).
5. Horn, R., Patlak, J. B. & Stevens, C. F. Sodium channels need not open before they inactivate. *Nature* **291,** 426–427 (1981).
6. Dumaine, R. *et al.* Ionic mechanisms responsible for the electrocardiographic phenotype of the Brugada syndrome are temperature dependent. *Circ. Res.* **85,** 803–809 (1999).
7. Veldkamp, M. W. *et al.* Two distinct congenital arrhythmias evoked by a multidysfunctional Na^+ channel. *Circ. Res.* **86,** E91–E97 (2000).
8. Deschenes, I. *et al.* Electrophysiological characterization of SCN5A mutations causing long QT (E1784K) and Brugada (R1512W and R1432G) syndromes. *Cardiovasc. Res.* **46,** 55–65 (2000).
9. Priori, S. G. *et al.* Genetic and molecular basis of cardiac arrhythmias: impact on clinical management parts I and II. *Circulation* **99,** 518–528 (1999).
10. Viswanathan, P. C., Shaw, R. M. & Rudy, Y. Effects of IKr and IKs heterogeneity on action potential duration and its rate dependence: a simulation study. *Circulation* **99,** 2466–2474 (1999).
11. Dominguez, G. & Fozzard, H. A. Influence of extracellular K+ concentration on cable properties and excitability of sheep cardiac Purkinje fibers. *Circ. Res.* **26,** 565–574 (1970).
12. Cascio, W. E., Johnson, T. A. & Gettes, L. S. Electrophysiologic changes in ischemic ventricular myocardium: I. Influence of ionic, metabolic, and energetic changes. *J. Cardiovasc. Electrophysiol.* **6,** 1039–1062 (1995).
13. Krishnan, S. C. & Antzelevitch, C. Sodium channel block produces opposite electrophysiological effects in canine ventricular epicardium and endocardium. *Circ. Res.* **69,** 277–291 (1991).
14. Yan, G. X. & Antzelevitch, C. Cellular basis for the Brugada syndrome and other mechanisms of arrhythmogenesis associated with ST-segment elevation. *Circulation* **100,** 1660–1666 (1999).
15. Alings, M. & Wilde, A. "Brugada" syndrome: clinical data and suggested pathophysiological mechanism. *Circulation* **99,** 666–673 (1999).
16. Brugada, P. & Brugada, J. Right bundle branch block, persistent ST segment elevation and sudden cardiac death: a distinct clinical and electrocardiographic syndrome. A multicenter report. *J. Am. Coll. Cardiol.* **20,** 1391–1396 (1992).
17. Priori, S. G., Napolitano, C., Giordano, U., Collisani, G. & Memmi, M. Brugada syndrome and sudden cardiac death in children. *Lancet* **355,** 808–809 (2000).
18. Schott, J. J. *et al.* Cardiac conduction defects associate with mutations in SCN5A. *Nature Genet.* **23,** 20–21 (1999).
19. Bezzina, C. *et al.* A single Na^+ channel mutation causing both long-QT and Brugada syndromes. *Circ. Res.* **85,** 1206–1213 (1999).
20. Johns, D. C., Nuss, H. B. & Marban, E. Suppression of neuronal and cardiac transient outward currents by viral gene transfer of dominant negative KV4.2 constructs. *J. Biol. Chem.* **272,** 31598–31603 (1997).
21. Kambouris, N. G. *et al.* Phenotypic characterization of a novel long QT syndrome mutation in the cardiac sodium channel. *Circulation* **97,** 640–644 (1998).
22. Luo, C. H. & Rudy, Y. A dynamic model of the cardiac ventricular action potential. I. Simulations of ionic currents and concentration changes. *Circulation Research* **74,** 1071–1096 (1994).
23. Zeng, J., Laurita, K. R., Rosenbaum, D. S. & Rudy, Y. Two components of the delayed rectifier K^+ current in ventricular myocytes of the guinea pig type. Theoretical formulation and their role in repolarization. *Circ. Res.* **77,** 140–152 (1995).
24. Davignon, A. *et al.* Normal ECG standards for infants and children. *Pediatr. Cardiol.* **1,** 123–152 (1979).

Acknowledgements

Financial support for this study was provided by the Interuniversity Cardiology Institute of Netherlands (H.L.T. and A.A.M.W.), the Dutch Heart Foundation (A.A.M.W.) and the NIH (J.R.B.) We thank S. Stepanovic and M. Hulsbeek for technical assistance, and L. DeFelice, D. Roden, M. Anderson and A. George for helpful discussion.

Correspondence and requests for materials should be addressed to J.R.B. (e-mail: jeff.balser@mcmail.vanderbilt.edu).

The voltage-sensitive sodium channel is a bell-shaped molecule with several cavities

Chikara Sato*, Yutaka Ueno*, Kiyoshi Asai*, Katsutoshi Takahashi†, Masahiko Sato‡, Andreas Engel§ & Yoshinori Fujiyoshi‖

* *Supermolecular Science Division, Electrotechnical Laboratory (ETL), Umezono 1-1-4, Tsukuba, 305-8568 Japan*
† *School of Knowledge Science, Japan Advanced Institute of Science and Technology Hokuriku (JAIST), Asahidai 1-1, Tatsunokuchi, Ishikawa, 923-1211, Japan*
‡ *Central Research Institute, Itoham Foods Inc., Kubogaoka 1-2, Moriya, 302-0104, Japan*
§ *Maurice E. Müller Institute, at the Biozentrum, University of Basel, Klingelbergstrasse 70, CH-4056 Basel, Switzerland*
‖ *Department of Biophysics, Faculty of Science, Kyoto University, Oiwake, Kitashirakawa, Sakyo-ku, Kyoto, 606-8502, Japan*

Voltage-sensitive membrane channels, the sodium channel, the potassium channel and the calcium channel operate together to amplify, transmit and generate electric pulses in higher forms of life. Sodium and calcium channels are involved in cell excitation, neuronal transmission, muscle contraction and many functions that relate directly to human diseases[1–4]. Sodium channels—glycosylated proteins with a relative molecular mass of about 300,000 (ref. 5)—are responsible for signal transduction and amplification, and are chief targets of anaesthetic drugs[6] and neurotoxins[1]. Here we present the three-dimensional structure of the voltage-sensitive sodium channel from the eel *Electrophorus electricus*. The 19 Å structure was determined by helium-cooled cryo-electron microscopy and single-particle image analysis of the solubilized sodium channel. The channel has a bell-shaped outer surface of 135 Å in height and 100 Å in side length at the square-shaped bottom, and a spherical top with a diameter of 65 Å. Several inner cavities are connected to four small holes and eight orifices close to the extracellular and cytoplasmic membrane surfaces. Homologous voltage-sensitive calcium and tetrameric potassium channels, which regulate secretory processes and the membrane potential[7], may possess a related structure.

Different approaches have provided information on the structure of the sodium channel. Its function and folding topology have been assessed by site-directed mutagenesis[8,9] and peptide-specific antibody binding[10,11]. The structure of a synthetic peptide

© 2001 Macmillan Magazines Ltd